



# Synthesizing, Characterization, and Electrochemical Behavior of $[(B-\alpha-SiW_9O_{34})_2Cd_4(H_2O)_2]^{12-}$ and Evaluating the Toxicity of this Compound and Other Sandwich-Type Polyoxometalates on Human Cancer Cell Lines by Inducing Apoptosis

Zahra Tayarani-Najaran, Nasrin Mohajeri, Aidin Mohammadi Zonouz, Farrokhzad Mohammadi Zonoz\*, Mehdi Baghayeri

Received: 08/01/2025 Resubmitted: 13/02/2025 Accepted: 10/03/2025 Published: 23/03/2025 DOI: 10.61186/MCH.2025.1077



## ABSTRACT

The dimeric silicotungstate,  $[(B-\alpha-SiW_9O_{34})_2Cd_4(H_2O)_2]^{12-}$  (**I**), has been synthesized in a new and simple method by reaction of  $A-b-Na_9HSiW_9O_{34} \cdot 23H_2O$  with cadmium nitrate under controlled temperature conditions. **I** was characterized by elemental analysis, FT-IR,  $^{29}Si$ , and  $^{113}Cd$  NMR spectroscopy, and this was verified by single-crystal X-ray structural analysis of the combined salts of  $Na^+$  and  $NH_4^+$ . The  $(NH_4)_{10}Na_2[(B-\alpha-SiW_9O_{34})_2Cd_4(H_2O)_2] \cdot 22H_2O$  salt crystallizes in the monoclinic system (space group  $P2_1/n$ ) with  $a = 16.2706(18) \text{ \AA}$ ,  $b = 13.8262(17) \text{ \AA}$ ,  $c = 20.307(3) \text{ \AA}$ ,  $\beta = 113.419(2)^\circ$  and  $Z = 2$ . Two lacunary  $B-\alpha-[SiW_9O_{34}]^{10-}$  Keggin moieties are connected by a rhomboid  $Cd_4O_{16}$  group to form the heteropolyanion, which has a sandwich-like shape. Cyclic voltammetry was used to examine the electrochemical and electrocatalytic properties of **I** in an aqueous solution. The redox processes of  $W^{VI}$  and  $Cd^{II}$  centers are represented by the two sequential cathodic/anodic peaks observed in electrochemical experiments. The redox waves of **I** are pH-dependent. For this compound, the tungsten and cadmium-centered waves exhibit a classical potential shift at pH values between 1.6 and 4.6 as a function of acidity. **I** electrocatalysis tendencies toward the reduction of nitrite ions have been thoroughly investigated. Additionally, in this study, the cytotoxic and apoptogenic activity of several sandwiched-type polyoxometalates (**I**,  $[(B-\alpha-PW_9O_{34})_2Cd_4(H_2O)_2]^{10-}$  (II),  $[(B-\alpha-PW_9O_{34})_2Mn_4(H_2O)_2]^{10-}$  (III),  $[(B-\alpha-PW_9O_{34})_2Co_4(H_2O)_2]^{10-}$  (IV),  $[(B-\alpha-PW_9O_{34})_2Zn_4(H_2O)_2]^{10-}$  (V),  $[(ZnW_9O_{34})_2WZn_3(H_2O)_2]^{12-}$  (VI),  $[(ZnW_9O_{34})_2WCd_3(H_2O)_2]^{12-}$  (VII), and  $[(B-\alpha-PW_9O_{34})_2Zn_2Cd_2(H_2O)_2]^{10-}$  (VIII)) were tested on four types of human cancer cells (MCF-7, B16F10, DU-145, and PC3). All tested compounds showed cytotoxic activity which is mediated via apoptosis.

## Keywords:

Sandwich-type polyoxometalates,  $^{113}Cd$  NMR spectroscopy,  $^{29}Si$  NMR spectroscopy, Electrochemistry, Cytotoxicity, Apoptosis



\*Corresponding author: f.zonoz@hsu.ac.ir; fmzonoz@gmail.com

This is an open access article published under the [CC BY 4 DEED](https://creativecommons.org/licenses/by/4.0/) license 

## INTRODUCTION

The possibility of using polyoxometalates (POMs) in catalysis, medicine, and material science has greatly sparked interest in the chemistry of these compounds [1–4]. Among these clusters, one of the most interesting groupings is the transition metal-substituted polyoxometalates (TMSPs). These compounds can be created by inserting a heteroatom (or, more frequently, substituting one or more addenda atoms) with lower valent transition metals. The Keggin and Wells-Dawson structures form the foundation for the most prevalent kinds of TMSPs [5, 6].

A subgroup of TMSPs has been investigated in recent years by research teams studying heteropolyanions. These compounds can be seen as having transition metals "sandwiched" between two trivacant forms of the parent Keggin or Wells-Dawson structures [7, 8]. As an illustration, a large number of tetra nuclear sandwich-type complexes  $[(M_4(H_2O)_2(PW_9O_{34})_2)]^{10-}$  (abbreviated as  $P_2W_{18}M_4$ ) are known with different divalent metal ions ( $M^{II} = Mn, Co, Cu, Zn, Cd$ ) [9, 10].

Recently, the possibilities of preparing dimeric or sandwiched compounds of heteropolyanions containing  $[SiW_9O_{34}]^{10-}$  unit were studied. Subsequently, the anions  $[Zr_3(H_2O)_2(SiW_9O_{34})_2]^{11-}$ ,  $[Si_2W_{18}Ti_6O_{77}]^{14-}$ ,  $[Cr_6(OH)_9(SiW_9O_{34})_2]^{11-}$  and  $[Sn_3(SiW_9O_{34})_2]^{14-}$  have been synthesized [11–14].

In 2000, Kortz et al. reported some tetra nuclear sandwiched-type complexes of silicotungstates based on the lacunary Keggin ion,  $[(SiW_9O_{34})_2M_4(H_2O)_2]^{12-}$  ( $M^{II} = Mn, Cu, Zn$ ) [15]. The synthesis of these compounds relies on the interaction between transition metal ions and  $[\gamma-SiW_{10}O_{36}]^{8-}$ . In 2013, Jiuyu Guo et al. discovered that the dimerization of  $[SiW_9O_{34}]^{10-}$  anions forms the open Wells-Dawson anion  $[Si_2W_{18}O_{66}]^{16-}$  [16]. Also, another sandwiched-type compounds based on  $[SiW_9O_{34}]^{10-}$  anions ( $TBA_7H_2[Ag_2(SiW_9O_{31})_2(CH_3COO)_3] \cdot H_2O \cdot CCl_4$  and  $[TBA_8H_6Ag_6(SiW_9O_{33})_2(DMF)]^{2+}$ ) reported by Kentaro Yonesato et al [17]. The use of POMs in reducing nitrite, iodate, hydrogen peroxide, and bromate has been the subject of numerous investigations during the past decades [18, 19]. Although most electrode surfaces require a significant overpotential for direct electro-reduction of nitrite ions, sandwich-type POMs have lately been able to reduce  $NO_2^-$  electro-catalytically with much less effort [20].

Cancer, one of the leading causes of death worldwide, encompasses a range of disorders in which cells grow uncontrollably, forming tumors or causing blood cancers, with the most common types being lung, colon, prostate, and breast cancer [21–23]. Even though cancer treatment has advanced over time, distant metastasis and tumor recurrence rates are still significant [24]. Conventional cancer treatment includes surgery, hormone therapy, radiation, and chemotherapy [25]. Chemotherapy is one of the most popular cancer therapies, with the main objective of eradicating and reducing the proliferation of cancer cells through the administration of one or more anticancer medications [26]. One of the primary mechanisms of action of chemotherapy may be the induction of apoptosis, a genetically set process that results in cells dying [27, 28]. The major drawbacks of chemotherapy drugs include severe side effects caused by a lack of selectivity, ineffectiveness against specific cancer types, and low absorption. Therefore, searching for alternative medications that selectively disable cancer cells without severely harming normal cells continues [21, 29].

Recently, along with the rapid development of the structures of the POMs, these compounds are ideally suited for biological applications owing to their promising anti-tumor [30–32], anti-viral [33, 34], anti-bacterial [35–37], anti-fungal [38, 39], anti-diabetes [40, 41], anti-Alzheimer's [41], skin anti-aging [42], and cancer diagnosis [30, 31] activities. Although the exact processes by which POMs exert their biomedical applications are not still clear, they probably catalyze Fenton-like reactions to increase ROS levels and possess anti-inflammatory and immunomodulatory properties [43–45]. POMs can also be used as biosensors [46, 47]. The first reports of anticancer, antiviral, and antibacterial activities of POMs were in 1965, 1971, and 1993, respectively [48]. Since then, many POMs, polyoxotungstates in particular, have been extensively studied for their activities *in vitro* [49].

In this work, we describe the synthesis and crystal structure of another member of sandwich-type polyoxometalates. This new cadmium-containing heteropolyanion was synthesized by a reaction of  $[A-SiW_9O_{34}]^{10-}$  unit which surrounds four cadmium. Besides the characterization of *I*, this compound's electrochemistry, electrocatalytic, and photocatalytic properties were studied. Additionally, AlamarBlue® cell proliferation assay was used to assess the cytotoxic activity of  $[(B-\alpha-SiW_9O_{34})_2Cd_4(H_2O)_2]^{12-}$  (*I*),  $[(B-\alpha-PW_9O_{34})_2Cd_4(H_2O)_2]^{10-}$  (*II*),  $[(B-\alpha-PW_9O_{34})_2Mn_4(H_2O)_2]^{10-}$  (*III*),  $[(B-\alpha-PW_9O_{34})_2Co_4(H_2O)_2]^{10-}$  (*IV*),  $[(B-\alpha-PW_9O_{34})_2Zn_4(H_2O)_2]^{10-}$  (*V*),  $[(ZnW_9O_{34})_2WZn_3(H_2O)_2]^{12-}$  (*VI*),

[(ZnW<sub>9</sub>O<sub>34</sub>)<sub>2</sub>WCd<sub>3</sub>(H<sub>2</sub>O)<sub>2</sub>]<sup>12-</sup> (VII), and [(B-α-PW<sub>9</sub>O<sub>34</sub>)<sub>2</sub>Zn<sub>2</sub>Cd<sub>2</sub>(H<sub>2</sub>O)<sub>2</sub>]<sup>10-</sup> (VIII) compounds, and Propidium iodide (PI) staining was used to examine the apoptotic effect of I, III, V, and VI POMs.

## EXPERIMENTAL

### Materials and Apparatus

Without any additional purification, all analytical-grade reagents were used just as they were obtained from commercial sources. [A—SiW<sub>9</sub>O<sub>34</sub>]<sup>10-</sup> was synthesized according to the literature and characterized by IR spectra [50]. FT-IR spectroscopy was used to characterize the S2-S8 compounds after they were synthesized by the published procedures [10, 51–54]. A KBr pellet was used to record FT-IR spectra on a Shimadzu 8400S FT-IR spectrophotometer within the 4000–400 cm<sup>-1</sup> range. The NMR spectrum was recorded on a Bruker BRX-300 AVANCE Spectrometer. The <sup>29</sup>Si and <sup>113</sup>Cd nuclei resonance frequencies are 99.36 and 110.92 MHz, respectively. Chemical shifts for <sup>29</sup>Si and <sup>113</sup>Cd NMR spectra were externally referenced relative to SiMe<sub>4</sub> and 0.1 M cadmium perchlorate, respectively. Elemental analyses were carried out in an Integra XL Inductively Coupled Plasma Spectrometer. All electrochemical analyses were performed using deionized water. The solutions were kept in N<sub>2</sub> atmosphere throughout the experiment and fully deaerated for at least 20 min using pure N<sub>2</sub> bubbles. The Metrohm 797VA computerized polarographic analyzer was used for the electrochemical setup. There was a standard three-electrode setup. Glassy carbon (GC) served as the working electrode. An Ag/AgCl (3 M KCl) electrode was the reference electrode, and a platinum electrode was the counter electrode. Every potential was recorded and measured with the Ag/AgCl electrode. Every voltammetric test was conducted at room temperature. For electrochemical investigations, 0.5 M buffer solutions of NaOAc/HOAc (pH = 4.6) and Na<sub>2</sub>SO<sub>4</sub>/H<sub>2</sub>SO<sub>4</sub> (pH = 1.6, 2.6, and 3.6) were prepared by combining different amounts of related acids and salts.

### Synthesis of Compound (NH<sub>4</sub>)<sub>10</sub>Na<sub>2</sub>[(B-α-SiW<sub>9</sub>O<sub>34</sub>)<sub>2</sub>Cd<sub>4</sub>(H<sub>2</sub>O)<sub>2</sub>]·22H<sub>2</sub>O (I)

I was synthesized as a new method in comparison to published work [55]. A 10.0 g (3 mmol) of [A—SiW<sub>9</sub>O<sub>34</sub>]<sup>10-</sup> was added in small portions with stirring to a solution of 3.08 g (10 mmol) of Cd(NO<sub>3</sub>)<sub>2</sub>·4H<sub>2</sub>O in 100 ml of distilled water. This suspension was heated at 50–60 °C for 3 h and then cooled to room temperature. All insoluble materials were filtered, and 15 g of potassium chloride was added to the solution. The mixture was stirred for 15 minutes and filtered off. This solid was recrystallized from 60 °C H<sub>2</sub>O and dried under vacuum. (Yield 1.16g, 13.6%). Elemental analysis for K<sub>12</sub>[Si<sub>2</sub>W<sub>18</sub>Cd<sub>4</sub>O<sub>68</sub>(H<sub>2</sub>O)<sub>2</sub>]·18H<sub>2</sub>O: Calcd: K, 8.18; Si, 0.98; W, 57.73; Cd, 7.84; H<sub>2</sub>O, 5.65 %. Found: K, 8.01; Si, 0.91; W, 57.61; Cd, 7.73; H<sub>2</sub>O, 5.51%. Using NH<sub>4</sub>Cl instead of KCl throughout the synthesis process, the crystals of ammonium salt suitable for crystallographic analysis were created. <sup>29</sup>Si NMR in D<sub>2</sub>O: δ -84.9 ppm. <sup>113</sup>Cd NMR in D<sub>2</sub>O: δ 53.40, and 87.75 ppm. Selected FT-IR bands in 1400–700 cm<sup>-1</sup> (KBr pellets): 987 (s), 949 (s), 893 (s), 846 (s), and 744 (s) cm<sup>-1</sup>.

### Preparation of I-CPE

To prepare I-CPE, 0.03 g of I powder and 0.02 g of graphite were combined and ground into a homogeneous mixture using an agate mortar and pestle. Subsequently, a glass rod was used to agitate the solid mixture after 0.4 mL of paraffin was added. A glass tube with a diameter of 0.8 mm was filled with the homogeneous mixture, and a copper wire was used to make an electrical connection to the electrode's back. By rubbing the electrode surface on the soft paper, the electrode's external surface was cleaned.

### Single Crystal Structure Description of I

A transparent I plate with dimensions of 0.20 x 0.15 x 0.03 mm<sup>3</sup> was employed for the X-ray work. Intensity measurements were taken at 110 K on a Bruker SMART 1000 CCD single crystal diffractometer with graphite-monochromated Mo Kα radiation (λ = 0.71073Å). A total of 12220 independent reflections (2θ<sub>max</sub> = 60.12° and R<sub>int</sub> = 0.0996) were recorded, of which 8862 reflections were considered [I > 2σ(I)]. The final cycle of refinement converged at R = 0.0658 and of RW = 0.1578 [I > 2σ(I)]. The intensities were corrected for Lorentz-polarization effects and the SADABS program [53] was applied for absorption correction. The structure was refined with SHELXL-97 [51] by full-matrix least-squares on F<sup>2</sup>. The weighting scheme was w = 1/[σ<sup>2</sup>(F<sub>o</sub><sup>2</sup>) + (0.1056P)<sup>2</sup>] where P = (F<sub>o</sub><sup>2</sup> + 2F<sub>c</sub><sup>2</sup>)/3.

## Cell Lines and Cell Cultures

Human breast cancer cell line (MCF-7), murine melanoma cell line (B16F10), and human prostate cancer cell lines (PC3 and DU145) were purchased from the Pasteur Institute (Tehran, Iran) and were kept at 37°C in a 90% humidified environment with 5% CO<sub>2</sub>. Cell lines were cultivated in 5% (v/v) fetal calf serum (FCS), 100 units/mL penicillin, and 100 µM streptomycin in Roswell Park Memorial Institute medium (RPMI). For each concentration and time course study, there was a control sample which remained untreated and received an equal volume of medium.

## Cell Proliferation Assay

Utilizing the reduction power of living cells, the active ingredient in alamarBlue®, resazurin, converts to resorufin, serving as a cell viability indicator. The reduction happens in the living cytosol of the cells. Resorufin is a reddish-colored, highly fluorescent molecule, while resazurin is a blue, practically non-fluorescent, non-toxic, cell-permeable substance. Viable cells constantly transform resazurin into resorufin, which intensifies the overall fluorescence and color of the media around the cells [56]. Around  $5 \times 10^3$  MCF-7, B16F10, PC3, and DU145 cells were cultured in each well of 96-microwell plate and incubated with different concentrations of each extract sandwich-type POMs. As directed by the manufacturer, alamarBlue® (10 mg/DI in PBS) was introduced to each well after a 48-hour incubation period. The cell viability was assessed after 4 hours in culture using a Synergy H4 Hybrid Multi-Mode Microplate Reader (BioTek, Winooski, USA) to measure the absorbance at 570 and 600 nm.

## PI Staining

PI staining of treated cells was used to identify apoptotic cells and flow cytometry was used to find the so-called sub-G1 peak [57, 58]. Little particles of DNA are produced during DNA fragmentation and can be eluted after being incubated in a hypotonic phosphate-citrate buffer. Cells lacking DNA will appear to the left of the G1 peak and will absorb less color when tagged with a quantitative DNA-binding dye like PI. Summarily,  $5 \times 10^4$  MCF-7 cells were placed in each well of a 24-well plate and subjected to different concentrations of the S1, S3, S5, and S6 for 48 h. Following the collection of floating and sticking cells, 400 µl of a hypotonic buffer (50 µg/ml PI in 0.1% sodium citrate plus 0.1% Triton X-100) was added, and the cells were incubated at 4°C overnight in the dark. The cells were then subjected to flow cytometric analysis using a FACScan flow cytometer (Partec GmbH, Münster, Germany).

## Statistical Analysis

Unless otherwise noted, all results are means ± SEM from triplicate tests carried out in parallel. One-way ANOVA was used to examine any statistical differences between the groups, and Bonferroni post hoc tests were then performed. The significance of the difference is denoted by the symbols \*P < 0.05, \*\*P < 0.01, and \*\*\*P < 0.001, and all comparisons were done in relation to untreated controls.

## RESULTS AND DISCUSSION

### Synthesis of *I*

The new Cd<sup>II</sup> substituted polyoxometalate, *I*, which can be separated in pure form as its NH<sub>4</sub><sup>+</sup> and K<sup>+</sup> salts, is produced via the reaction of [A-SiW<sub>9</sub>O<sub>34</sub>]<sup>10-</sup> in an aqueous solution with Cd<sup>2+</sup> ions. In 2011, Lijuan Chen et al. synthesized silicotungstate sandwich-type dimer K<sub>18</sub>{[Mn(H<sub>2</sub>O)<sub>3</sub>]<sub>2</sub>[Mn(H<sub>2</sub>O)<sub>2</sub>]}[(B-β-SiW<sub>9</sub>O<sub>33</sub>(OH))Mn<sub>3</sub>(H<sub>2</sub>O)(B-β-SiW<sub>8</sub>O<sub>30</sub>(OH))]<sub>2</sub> · 16H<sub>2</sub>O by [γ-SiW<sub>10</sub>O<sub>36</sub>]<sup>8-</sup> ions as a primary compound. This reaction must involve rotational isomerization of [γ-SiW<sub>10</sub>O<sub>36</sub>]<sup>8-</sup> (γ β lacunary Keggin) [59]. This is an interesting outcome since the formation of *I* involves the rotational isomerization of A-SiW<sub>9</sub>O<sub>34</sub> to B-α-SiW<sub>9</sub>O<sub>34</sub> followed by cadmium insertion. We found that the [SiW<sub>12</sub>O<sub>40</sub>]<sup>4-</sup> anion was the predominant product when solutions of

*I* was passed through a strongly acidic ion exchange column (or was maintained under acidic conditions with pH < 1). Some sandwich-type heteropolyanions show this behavior[54]. This homology is an indirect cue that the skeletal arrangement of the *I* silicotungstate sandwich-type dimer is comparable to a Keggin structure.

## X-Ray Single-Crystal Structure Analysis of the $\text{NH}_4^+$ Salt

Table 1 lists the structural refinement parameters and crystallographic data. The single crystal analysis shows that the crystalline *I* is crystallized in the diagonal space group P2(1)/n (No. 14).

**Table 1.** Important crystal refinement parameters of  $(\text{NH}_4)_{10}\text{Na}_2[\text{Cd}_4(\text{H}_2\text{O})_2(\text{SiW}_9\text{O}_{34})_2]\cdot 22\text{H}_2\text{O}$

Empirical formula	$\text{H}_{88}\text{Cd}_4\text{N}_{10}\text{Na}_2\text{O}_{92}\text{Si}_2\text{W}_{18}$
Formula weight	5561.86
Temperature(K)	110(2)
Wavelength	0.71073
Space group	P2(1)/n (No. 14)
Unit cell dimensions	a = 16.2706(18) Å $\alpha = 90^\circ$ b = 13.8262(17) Å $\beta = 113.419(2)^\circ$ c = 20.307(3) Å $\gamma = 90^\circ$
Volume	4192.1(9) Å <sup>3</sup>
Z	2
Density(calc)	4.406 Mg/m <sup>3</sup>
Absorption coefficient	25.745 mm <sup>-1</sup>
Reflections collected	49812
Independent reflections	12220 [ $R_{\text{(int)}} = 0.0996$ ]
Reflections ( $I > 2\sigma(I)$ )	8862
Data / restraints / parameters	12220 / 0 / 577
Goodness of fit on $F^2$	0.982
Largest diff. peak and hole	5.001 and $-3.474 \text{ e.}\text{\AA}^{-3}$
Final R indices	$R(F_0)^a = 0.0658$ $R_w(F_0)^b = 0.1578$

$$^a R = \sum ||F_0| - |F_c|| / \sum |F_0|.$$

$$^b R_w = [\sum w(F_0^2 - F_c^2)^2 / \sum (F_0^2)^2]^{1/2}.$$

In Figure 1A, the structure of *I* is displayed. Two (B- $\alpha$ - $\text{SiW}_9\text{O}_{34}$ ) ligands are presented in the anion, connected by a  $\text{Cd}_4\text{O}_{16}$  unit made up of four edge-sharing  $\text{CdO}_6$  octahedra. This structure is the same of  $\{[\text{SiM}_2\text{W}_9\text{O}_{34}(\text{H}_2\text{O})]_2\}^{12-}$  ( $M = \text{Mn}^{2+}$ ,  $\text{Cu}^{2+}$ , and  $\text{Zn}^{2+}$ ) and  $[(\text{B-}\alpha\text{-PW}_9\text{O}_{34})_2\text{Cd}_4(\text{H}_2\text{O})_2]^{10-}$  which was previously reported [10, 15]. The unit cell of *I* is shown in Figure 1B. Two  $\text{Na}^+$  cations connect with the two terminal oxygen atoms of *I*. (O34 in each half of the B- $\alpha$ - $\text{SiW}_9\text{O}_{34}$  unit in *I*). The average distance between these  $\text{Na}^+$  ions and oxygen atoms is 2.426 Å (Table S1, Supporting Information). The  $\text{Na}^+$  ions can be considered linked to the oxygen by comparing this distance to other bond lengths in *I*. Figure 1C provides an overview of the relevant angles and distances for the  $\text{Cd}_4\text{O}_{16}$  unit of *I* and II. As can be seen, the values of bond lengths of Cd cations in the  $\text{Cd}_4\text{O}_{16}$  unit for II are greater than *I* due to the larger size of the phosphorus atoms.

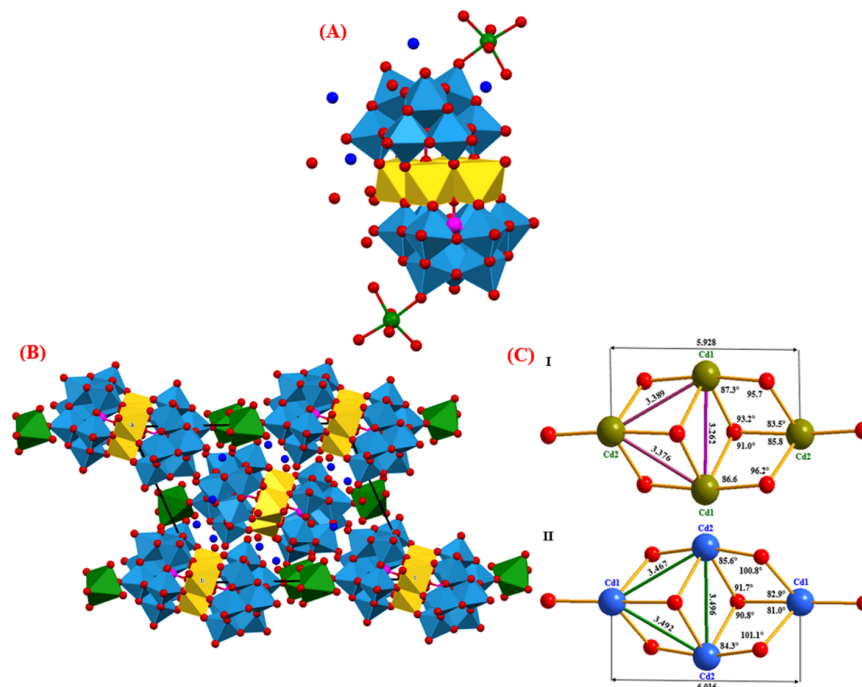


**Figure 1.** A) The molecular structure of I, B) The unit cell of I, and C) Relevant distances (Å) and angles (°) for the  $\text{Cd}_4\text{O}_{16}$  unit of I and II compounds.

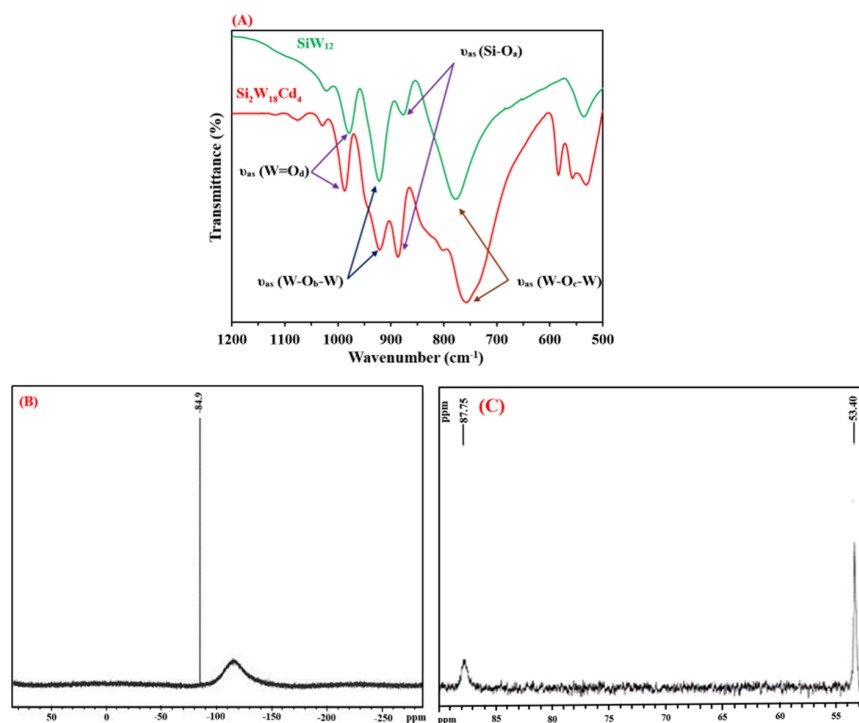


**Figure 2.** A) FT-IR spectra of *I* (red) and  $[\text{SiW}_{12}\text{O}_{40}]^{4-}$  (green), B)  $^{29}\text{Si}$  NMR, and C)  $^{113}\text{Cd}$  NMR spectra of *I*

### FT-IR, $^{29}\text{Si}$ and $^{113}\text{Cd}$ NMR Spectroscopy

The FT-IR spectra of  $[\text{SiW}_{12}\text{O}_{40}]^{4-}$  and *I* are compared in Figure 2A. Five bands are observed in the FT-IR spectrum of  $[\text{SiW}_{12}\text{O}_{40}]^{4-}$  at 1020, 973, 922, 875, and 775  $\text{cm}^{-1}$ . On the other hand, the IR spectrum of *I* shows six bands at 987, 949 (sh), 920, 893, 802, and 755  $\text{cm}^{-1}$ . The broad bands of  $[\text{SiW}_{12}\text{O}_{40}]^{4-}$  at 775  $\text{cm}^{-1}$  split into two bands at 802 and 755  $\text{cm}^{-1}$ . It is due to the reduction of symmetry in *I*. The FT-IR spectra of  $[\text{PW}_{12}\text{O}_{40}]^{3-}$  and  $[[(\text{B}-\alpha$

$\text{PW}_9\text{O}_{34})_2\text{M}_4(\text{H}_2\text{O})_2]^{10-}$  ( $\text{M} = \text{Co}^{2+}, \text{Cu}^{2+}, \text{and Zn}^{2+}$ ) also show this similarity [51]. These bands are related to the  $\text{SiO}_4$  tetrahedron,  $\text{W} = \text{O}$  (terminal), and  $\text{W-O-W}$  (corner and edge-sharing  $\text{WO}_6$  octahedra) [55].

One peak at  $-84.9$  ppm is observed in the  $^{29}\text{Si}$  NMR spectrum of *I*, indicating that there is just one type of silicon present in the dimeric compound (Figure 2B). This pattern shows a single and highly pure product. This peak is assigned to the central  $\text{SiO}_4$  unit of the silicotungstate [60]. The  $^{29}\text{Si}$  NMR chemical shift patterns for some silicotungstate sandwich-type polyoxometalates are shown in Table 2.

**Table 2.**  $^{29}\text{Si}$  NMR chemical shift patterns for some silicotungstate sandwich-type polyoxometalates

compound	$\delta$ ( $^{29}\text{Si}$ NMR), ppm	ref.
$\alpha\text{-Si}_2\text{W}_{18}(\text{PhSnOH})_3$	-83.2	[13]
$\alpha\text{-Si}_2\text{W}_{18}(\text{BuSnOH})_3$	-82.3	[13]
$\beta\text{-Si}_2\text{W}_{18}(\text{PhSnOH})_3$	-82.4	[13]
$\beta\text{-Si}_2\text{W}_{18}(\text{ZrOH})_3$	-84.2	[12]
$\alpha\text{-Si}_2\text{W}_{18}\text{Sn}^{\text{II}}_3$	-85.2	[13]
$\beta\text{-Si}_2\text{W}_{18}\text{Sn}^{\text{II}}_3$	-85.0	[13]
$\text{Ag}_2(\text{SiW}_9\text{O}_{31})_2(\text{CH}_3\text{COO})_3$	-83.6	[17]
<b>I</b>	-84.9	This work

There are two prominent peaks in the  $^{113}\text{Cd}$  NMR spectra of *I* (Figure 2C) at 53.3986 and 87.7500 ppm. This pattern is consistent with single-crystal evidence, indicating that the *I* includes two forms of cadmium. In *I* anions,  $\text{Cd}_4\text{O}_{14}(\text{H}_2\text{O})_2$  bridges join two  $\text{B-}\alpha\text{-SiW}_9\text{O}_{34}$  units and there are two types of  $\text{Cd}^{2+}$  ions in the  $\text{Cd}_4\text{O}_{14}(\text{H}_2\text{O})_2$  fragment. One form, which consists of two Cd atoms, is entirely coordinated by oxygen atoms, whereas the other also has  $\text{H}_2\text{O}$  molecules as ligands. It is possible to explain the peak broadening and its multiplicity by the indirect spin-spin interaction of the  $^{29}\text{Si}$  and  $^{113}\text{Cd}$  nuclei through  $\text{Cd-O-Si}$  and  $\text{Cd-O-Cd}$  bonds. Similarly, the  $^{113}\text{Cd}$  NMR spectrum of  $[(\text{B-}\alpha\text{-PW}_9\text{O}_{34})_2\text{Cd}_4(\text{H}_2\text{O})_2]^{10-}$  displays two peaks at 26.25 and 52.76 ppm. The difference in values between the  $^{113}\text{Cd}$  NMR of the two compounds is related to the more negative charge of *I* composition compared to  $[(\text{B-}\alpha\text{-PW}_9\text{O}_{34})_2\text{Cd}_4(\text{H}_2\text{O})_2]^{10-}$  compound.

### Electrochemical Behavior of I

The cyclic voltammogram of *I* in acetate buffer solution ( $\text{pH} = 3.6$  and  $4.6$ ) is shown in Figure 3. In  $\text{pH} = 4.6$  (Figure 3A), the very strong quasi-reversible redox wave appears in the half-wave potential  $E_{1/2} = -0.86$  V  $\{E_{1/2} = (E_{p_a} + E_{p_c})/2\}$ . In voltammogram of *I* at  $\text{pH} = 3.6$  (Figure 3B), several quasi-reversible waves can be seen at potentials  $E_{1/2} = -0.6$ -,  $-0.73$ , and  $0.80$  V. The oxidation and reduction peaks related to  $E_{1/2} = -0.6$  V ( $\text{W}^{\text{VI}} \rightarrow \text{W}^{\text{V}}$ ),  $-0.73$  V ( $\text{W}^{\text{VI}} \rightarrow \text{W}^{\text{V}}$ ;  $\text{Cd}^{\text{II}} \rightarrow \text{Cd}$ ), and  $-0.83$  V ( $\text{W}^{\text{VI}} \rightarrow \text{W}^{\text{V}}$ ). According to Fig. 3C and the fact that the oxidation-reduction potentials of cadmium and tungsten ions are observed at negative potentials, it can be said that these waves are related to the oxidation-reduction reactions of cadmium and tungsten centers that overlapped with each other. It can also be noted that these waves are pH-dependent.

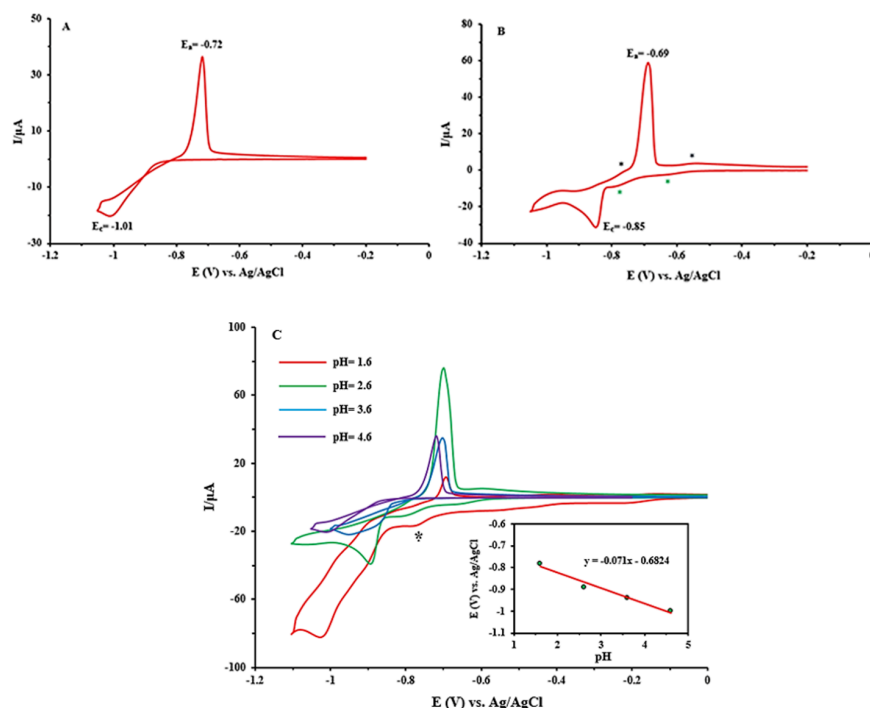
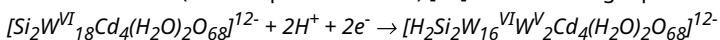


**Figure 3.** Cyclic voltammograms (scan rate:  $50 \text{ mV s}^{-1}$ ) of *I-CPE* in A) pH = 4.6 and B) pH = 3.6. (Buffer solution of NaOAc/HOAc) and C) at various pH values (from down to top: 1.6, 2.6, 3.6, and 4.6) with scan rate  $50 \text{ mV s}^{-1}$ . Inset: the relationship between peak potentials of wave versus pH.

POMs typically undergo protonation in conjunction with reduction, which means that their electrochemical activity is pH-dependent. Figure 3C presents the CV changes of *I-CPE* as a function of pH. Over the pH range of 1.6–4.6 in buffer solution, wave currents decrease and all wave potentials eventually shift toward negative potential as the pH rises. The Nernst equation explains these observations. The linear relationship between the corresponding redox potential and pH is displayed in the inset of Figure 3C. The wave slope is  $-71 \text{ mV/pH}$ , which is equal to the transfer of approximately two protons per two-electron reduction of tungsten and cadmium centers in comparison with the theoretical value ( $-59 \text{ mV/pH}$  for  $2e^-/2H^+$ ) [61]. The following equation explains this for *I*:



#### Electrocatalysis of NO<sub>2</sub>- Reduction by *I-CPE*

The results of the nitrite reduction study have several wider implications, especially for environmental research, public health, and agricultural methods. Water bodies frequently contain nitrite, a pollutant that comes from wastewater or agricultural runoff. These problems can be minimized, and hazardous nitrite can be changed into less dangerous forms by using POMs for nitrite reduction. Many studies have been conducted on the reduction of nitrite ion by Keggin structures, but no reports have been presented on sandwich polyoxometalates. The important point is that Keggin compounds are stable at low pH, but the compound used is stable at high pH [61].

Research on the electrocatalytic characteristics of *I-CPE* has revealed that the compound possesses appropriate electrocatalytic activities for the reduction of nitrate ions, which are associated with tungsten and cadmium centers. HNO<sub>2</sub> can slowly disproportionate under the below reaction:



To ensure that the influence of this reaction is minimal, experimental data relevant to nitrite catalysis were always obtained from freshly prepared solutions. According to previous work and based on using the differential electrochemical mass spectrometry (DEMS) technique, the reaction of HNO<sub>2</sub> or NO<sub>2</sub> with the reduced POM produces the gaseous products (NO and N<sub>2</sub>O). Only NO is detected by the POM's initial one-electron reduction procedure. However, N<sub>2</sub>O is produced along with NO when the POM is reduced by two electrons [62].

Because *I-CPE* should be an excellent candidate for this catalytic impact, we investigated its electrocatalytic activity on nitrite reduction at various pH values. Measurements must be done as soon as nitrite ions are added since a longer waiting period reduces the catalytic effect of POMs. In Figure 4A, the electrocatalytic activities of *I-CPE* in the reduction of nitrite ions are studied. We find that upon adding  $\text{NO}_2^-$ , the reduction current at the carbon paste electrode noticeably increased in the presence of *I* and the oxidation peak current decreased, while the naked glassy carbon does not show any response to  $\text{NO}_2^-$  ion. This behavior shows that nitrite ions can be catalyzed by *I* [63].

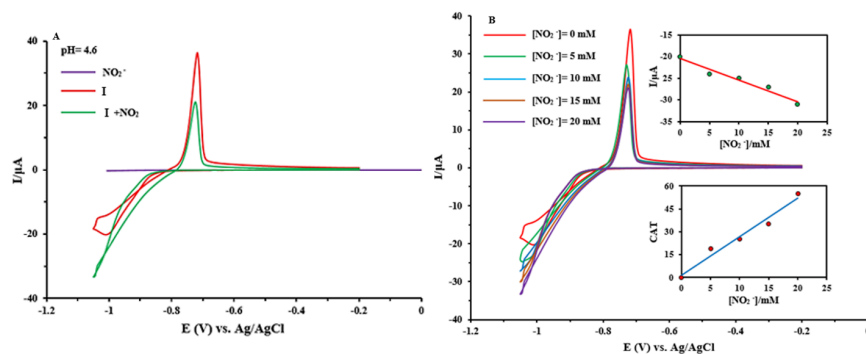


**Figure 4.** A) Cyclic voltammograms (scan rate  $50 \text{ mV s}^{-1}$ ) for  $\text{NO}_2^-$  solution, naked *I-CPE*, and *I-CPE* in the presence of  $\text{NO}_2^-$  (The 0.5 M buffer solutions of NaOAc/HOAc; pH = 4.6). B) Cyclic voltammograms of compound *I* in the reduction of nitrite ions. Insets: the relationship between cathodic wave current and CAT versus nitrite concentration

As illustrated in Figure 4B, when the sodium nitrite was increased, the cathodic current increased and the anodic current reduced until the anodic wave disappeared. This behavior suggests that nitrite ions are being reduced electrocatalytically, as would be expected from an electrocatalytic reaction. The catalytic efficiency of POM is defined by  $\text{CAT} = \frac{[I_c(\text{POM}, \text{NaNO}_2) - I_c(\text{POM})]}{I_c(\text{POM})} \times 100$  where  $I_c(\text{POM})$  and  $I_c(\text{POM}, \text{NaNO}_2)$  are the cathodic peak currents in the absence and the presence of nitrite ion, respectively [64]. The maximum calculated values of CAT for the last wave and highest  $\gamma$  at pH = 4.6 were obtained at 55% for *I*. This result suggested that *I* is a good electrocatalyst for  $\text{NO}_2^-$  ions.

### Cytotoxicity of Various POMs

The cytotoxic potential of substances I-VIII was examined on MCF-7, B16F10, PC3, and DU145 cells. The viability percentages of various concentrations of I-VIII POMs are given in Table 3. As demonstrated, POMs VI, VII, V, and III exhibit the lowest viability percentages at a concentration of 500  $\mu\text{g/ml}$  in MCF-7, B16-F10, PC-3, and DU-145 cell lines, respectively. All investigated POMs had lower IC50s than 1  $\mu\text{M}$  in the MCF-7 cell line which were also lower than the doxorubicin (DOX) IC50 value. II-VIII had IC50 values less than 1  $\mu\text{M}$  in the B16F10 cell line. The IC50 for I-III and V was less than 1  $\mu\text{M}$  in the PC3 cell line. Although all of the IC50 values of tested POMs were higher than DOX IC50 value in the B16F10 and PC3 cell lines. In the DU145 cell line, all of the evaluated POMs' had IC50 levels lower than 1  $\mu\text{M}$  and among them the IC50 values of I and II POMs were lower than DOX IC50 value. Table 4 contains the IC50 values for I-VIII components.

**Table 3.** Viability percentages of four cell lines treated with various concentrations of I-VIII POMs.

<b>Viability (%) ± SEM in different cell lines</b>					
	<b>Concentration (µg/ml)</b>	<b>MCF-7</b>	<b>B16-F10</b>	<b>PC-3</b>	<b>DU-145</b>
<b>I</b>	20	47.8 ± (4.6)	60.4 ± (0.8)	56.4 ± (5.4)	27.5** ± (0.9)
	100	33.5 ± (3.9)	52.6* ± (6.1)	52.4* ± (1.4)	17.8** ± (3.9)
	500	25.8* ± (1.2)	28.6* ± (1.1)	28.7** ± (2.0)	9.1** ± (2.8)
<b>II</b>	<b>Concentration (µg/ml)</b>	<b>MCF-7</b>	<b>B16-F10</b>	<b>PC-3</b>	<b>DU-145</b>
	20	44.9 ± (2.0)	35.9* ± (1.2)	63.1 ± (1.5)	30.4** ± (4.2)
	100	33.3* ± (1.7)	25.2* ± (4.0)	51.8* ± (1.3)	20.7** ± (0.8)
	500	30.3* ± (1.6)	5.7* ± (2.4)	13.1 ± (19.3)	12.3*** ± (1.1)
<b>III</b>	<b>Concentration (µg/ml)</b>	<b>MCF-7</b>	<b>B16-F10</b>	<b>PC-3</b>	<b>DU-145</b>
	20	40.1* ± (0.7)	49.5* ± (1.1)	57.4* ± (3.6)	27.2* ± (8.1)
	100	34.8 ± (3.1)	35.7 ± (9.3)	27.2* ± (0.7)	21.2*** ± (2.3)
	500	30.0* ± (1.7)	13.5* ± (4.2)	4.7*** ± (7.1)	4.2** ± (5.1)
<b>IV</b>	<b>Concentration (µg/ml)</b>	<b>MCF-7</b>	<b>B16-F10</b>	<b>PC-3</b>	<b>DU-145</b>
	20	42.0* ± (1.6)	43.0* ± (1.5)	84.2 ± (2.0)	38.9* ± (5.9)
	100	34.5 ± (6.0)	40.1* ± (0.2)	65.9* ± (2.5)	16.1** ± (3.8)
	500	20.3* ± (3.1)	25.9* ± (6.0)	51.6** ± (6.9)	14.4 ± (23.5)
<b>V</b>	<b>Concentration (µg/ml)</b>	<b>MCF-7</b>	<b>B16-F10</b>	<b>PC-3</b>	<b>DU-145</b>
	20	59.0 ± (6.6)	47.9* ± (1.6)	47.3* ± (1.1)	44.6* ± (4.1)
	100	39.3 ± (5.9)	44.7* ± (1.3)	26.8** ± (1.4)	26.7** ± (1.0)
	500	22.1 ± (6.1)	16.4* ± (2.5)	3.3* ± (9.7)	21.7*** ± (0.7)
<b>VI</b>	<b>Concentration (µg/ml)</b>	<b>MCF-7</b>	<b>B16-F10</b>	<b>PC-3</b>	<b>DU-145</b>
	20	16.5 ± (3.5)	58.3* ± (0.1)	74.0 ± (1.8)	48.5** ± (1.6)
	100	8.9 ± (5.0)	29.3* ± (1.4)	48.5* ± (2.5)	41.7* ± (3.9)
	500	2.4* ± (2.8)	4.9* ± (1.6)	22.0* ± (4.6)	25.8 ± (17.9)
<b>VII</b>	<b>Concentration (µg/ml)</b>	<b>MCF-7</b>	<b>B16-F10</b>	<b>PC-3</b>	<b>DU-145</b>
	20	38.3 ± (5.5)	65.9 ± (3.6)	67.6 ± (3.3)	40.7* ± (7.7)
	100	20.6 ± (6.6)	37.7** ± (6.9)	49.2* ± (1.2)	30.2* ± (5.7)
	500	6.6 ± (5.2)	4.7*** ± (5.4)	26.9 ± (18.5)	17.1* ± (7.9)
<b>VIII</b>	<b>Concentration (µg/ml)</b>	<b>MCF-7</b>	<b>B16-F10</b>	<b>PC-3</b>	<b>DU-145</b>
	20	45.9 ± (5.3)	59.9* ± (2.1)	95.3 ± (3.7)	47.0** ± (2.1)
	100	36.4 ± (4.8)	27.7* ± (7.1)	80.5 ± (2.9)	26.0** ± (2.3)
	500	34.1 ± (4.0)	7.8** ± (3.1)	51.8 ± (10.9)	8.8* ± (12.7)

\* P value < 0.05; \*\* P value < 0.01; \*\*\* P value < 0.001

**Table 4.** IC50 values for I–VIII POMs

	IC50 (μM)								DOX (reference)
	I	II	III	IV	V	VI	VII	VIII	
MCF-7	0.509	0.373	0.199	0.411	0.819	0.152	0.404	0.379	1.189 [65]
B16-F10	1.005	0.369	0.623	0.401	0.628	0.695	0.817	0.725	0.023 [66]
PC-3	0.917	0.934	0.703	2.100	0.575	1.096	1.050	2.041	0.240 [67]
DU-145	0.205	0.213	0.251	0.404	0.458	0.576	0.375	0.551	0.250 [68]

### Apoptosis Induction by I, III, V, and VI

Using PI staining test and flow cytometry, apoptosis in MCF-7 cell lines was identified. For 48 hours, cells were treated with different concentrations of I, III, V, and VI (25 μg/ml and 50 μg/ml). The induction of apoptosis in treated cells was demonstrated by the comparison of the Sub-G1 peak in flow cytometry histograms between treated cells and untreated control cells (= Sub-G1 peak). The flow cytometry histograms are shown in Figure 11.

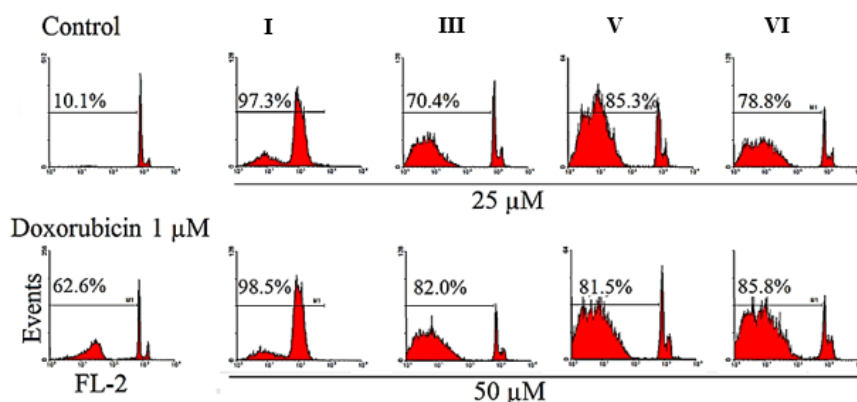


**Figure 11.** The flow cytometry histograms of unincubated and incubated cells with DOX (1 μM), I, III, V, and VI (25 and 50 μM) for 48 h

Apoptosis can be induced through multiple pathways, including effects on the cell cycle, protein expression, mitochondrial activity, reactive oxygen species (ROS) generation, and overall cell viability [69].

In 2013, Wang and colleagues investigated the anticancer effects of the dimanganese(II)-containing 20-tungsto-2-bismuthate (III)-based POM-dimer salt  $(\text{Himi})_2\text{Na}_4[(\text{Mn}(\text{H}_2\text{O})_3)_2(\text{W}(\text{OH})_2)_2(\text{BiW}_9\text{O}_{33})_2]\cdot 30\text{H}_2\text{O}$  ( $\{\text{MnBi}\}$ ) on gastric cancer SGC-7901 cells. Their findings showed that  $\{\text{MnBi}\}$  inhibited cell proliferation and induced apoptosis in a dose-dependent manner. Moreover, treatment with  $\{\text{MnBi}\}$  led to a reduction in the expression of bcl-2 and nuclear factor- $\kappa\text{B}$  p65 proteins, which are associated with cell survival and inflammation [70]. In 2014, Leon et al. found that  $[\text{Cu}_4(\text{H}_2\text{O})_2(\text{PW}_9\text{O}_{34})_2]\cdot 20\text{H}_2\text{O}$  triggers apoptosis in MG-63 osteosarcoma cells by increasing ROS levels, lowering the GSH/GSSG ratio, and inducing G2 phase cell cycle arrest in a dose-dependent manner (25–100 μmol/L). Notably, it demonstrated a stronger antiproliferative effect on MG-63 cells ( $\text{IC}_{50} = 22$  μmol/L) compared to normal osteoblasts ( $\text{IC}_{50} = 92$  μmol/L) and outperformed cisplatin in its effectiveness [71]. In 2018, Zhao et al. showed that another sandwich-type POM  $(\{\text{Na}_{0.7}\text{Ni}_{5.3}(\text{H}_2\text{O})_2(\text{imi})_2(\text{Himi})(\text{SbW}_9\text{O}_{33})_2\})^{6-}$  (imi = imidazole) was extremely cytotoxic against gastric cancer cells (AGS and BGC-823) by interrupting the cell cycle in the S-phase and triggering cell apoptosis [32]. In 2018, Luo et al. revealed that  $\text{Na}_2\text{K}_{0.5}\text{Sm}_{0.5}[\text{Sm}(\text{H}_2\text{O})_8][\text{K}_3\text{Cu}_2\text{WO}(\text{H}_2\text{O})_{10}][\text{B}-\alpha\text{AsW}_9\text{O}_{33}]\cdot 14\text{H}_2\text{O}$  may cause HepG2 cells and HCT-116 cells to undergo autophagy through the participation of lysosomes and apoptosis through the activation of caspase-3 in both cases [72]. In 2019, Wang et al. evaluated the anti-tumor activity of  $[\text{Na}(\text{H}_2\text{O})_4][\{\text{Na}_3(\text{H}_2\text{O})_5\}\{\text{Mn}_3(\text{bpp})_3\}(\text{SbW}_9\text{O}_{33})_2]\cdot 8\text{H}_2\text{O}$  (bpp = 1,3-bis(4-pyridyl) propane) *in vitro* and *in vivo*. They observed that this sandwich-type POM could inhibit the proliferation of human cancer cell lines, including SGC-7901, HT-29, HepG2,

Hela, U2OS, SaoS2, and HMC cells, and also suppress the development of tumor xenograft in mice, induce cell apoptosis, and release cytochrome c [73]. Consequently, the substances in this study may demonstrate their cytotoxicity activity in cancer cell lines by inducing apoptosis.

## CONCLUSION

---

In this work, we have successfully synthesized the  $(\text{NH}_4)_{10}\text{Na}_2[(\text{SiW}_9\text{O}_{34})_2\text{Cd}_4(\text{H}_2\text{O})_2]\cdot 22\text{H}_2\text{O}$  (*I*) in a simple method. This compound was characterized by routine techniques and then its structure was confirmed by single-crystal X-ray diffraction. Single-crystal X-ray diffraction,  $^{29}\text{Si}$  NMR, and  $^{113}\text{Cd}$  NMR spectroscopy prove the presence of silicon and cadmium atoms in the *I* compound. The redox wave of the cadmium and tungstate centers are pH-dependent. Over the pH range of 1.6 - 4.6 in buffer solution, the redox wave moves in the negative direction as the pH increases. The study of electrochemical and electrocatalytic properties exhibits that *I* have good electrocatalytic activity in the reduction of  $\text{NO}_2^-$ .

According to the results obtained from this study, it seems that I-VIII POMs have shown considerable cytotoxicity on MCF-7, B16F10, DU-145, and PC3 cell lines. *I*, III, V, and VI compounds were investigated for their ability to induce apoptosis. It was discovered that these compounds significantly affected apoptosis induction and could be employed as a potential chemotherapeutic drug.

## APPENDIX A

---

Crystallographic data for structural analysis *I* have been deposited with the Cambridge Crystallographic Data Center, CCDC No. 859177. Copies of this information may be obtained free of charge from the Director, CCDC, 12 Union Road, Cambridge CB2 1EZ, UK (Tel: +44 (0)1223 762911; e-mail: [deposit@ccdc.cam.ac.uk](mailto:deposit@ccdc.cam.ac.uk) or www: <http://www.ccdc.cam.ac.uk>).

## STATEMENTS AND DECLARATIONS

---

### Authors' Contributions

All authors contributed to data analysis, drafting, and revising of the paper and agreed to be responsible for all the aspects of this work.

### Competing Interests

The authors declare no competing interest.

### Ethics Approval

Not applicable.

### Data Availability

Data will be made available on request

### Funding

This paper received no external funding.

## AUTHORS' INFORMATION

---

**Zahra Tayarani-Najaran**—Department of Pharmacodynamics and Toxicology, School of Pharmacy; Mashhad University of Medical Sciences, Mashhad, Iran.

**Nasrin Mohajeri**—Samen Pharmaceutical Company, Mashhad, Iran.

**Aidin Mohammadi Zonouz**—Student Research Committee, Mashhad University of Medical Sciences, Mashhad, Iran.

**Farrokhzad Mohammadi Zonoz**—Department of Chemistry, Faculty of Science, Hakim Sabzevari University, Sabzevar, Iran.

**Mehdi Baghayeri**—Faculty of Chemistry, Silesian University of Technology, 44-100 Gliwice, Poland; Research Core of Advance Photo-electro Materials (APEM), Faculty of Science, Hakim Sabzevari University, Iran.

## REFERENCES

- [1] M.H. Alizadeh, H. Razavi, F. Farrash Bamoharram, M.K. Hassanzadeh, R. Khoshnavazi, F. Mohammadi Zonoz, Novel Catalytic Acetylation of Alcohols with Preyssler's Anion,  $[\text{NaP}_5\text{Wa}_{30}\text{O}_{110}]^{14-}$  Kinet. Catal., 44 (2003) 524-528.
- [2] F. Hajizadeh, F. Mohammadi Zonoz, S. Duval, B. Maleki, A. Amiri, Synthesis and investigation of two new crystal alline organic inorganic nano-hybrids based on Wells-Dawson vanadotungstates and 1H-1, 2, 4-triazole as electro- and photocatalysts, J. Mol. Struct., 1224 (2021) 129003.
- [3] S.S. Hosseinyzade, F.M. Zonoz, B. Bahramian, Nanohybrid Complexes with Molybdenyl Acetylacetonate, Schiff Base and Lacunary Keggin-Type Polyoxometalates: Synthesis and Catalytic Epoxidation of Olefins in the Presence of tert-Butyl Hydroperoxide, Catal. Letters, 148 (2018) 1324-1335.
- [4] X. Li, X. Liu, Y. Tao, W. Feng, H. Wang, M. Xu, Y. Sun, T. Sun, Polyoxometalate Nanomaterials for Tumor Phototherapy, ChemistrySelect, 10 (2025) e202405001.
- [5] S. Chang, Y.-F. Qi, E.-B. Wang, Z. Zhang, Two novel sandwiched-type polyoxotungstates containing Zn6 transition-metal cluster: Syntheses, structures and luminescent property, Inorganica Chim. Acta, 362 (2009) 453-457.
- [6] Y. Saku, Y. Sakai, K. Nomiya, Relation among the 2: 2-, 1: 1-and 1: 2-type complexes of hafnium (IV)/zirconium (IV) with mono-lacunary  $\alpha_2$ -Dawson polyoxometalate ligands: Synthesis and structure of the 2: 2-type complexes  $[\{\alpha_2\text{-P}_2\text{W}_{17}\text{O}_{61}\text{M}(\mu\text{-OH})(\text{H}_2\text{O})\}_2]^{14-}$  (M= Hf, Zr), Inorg. Chim. Acta., 363 (2010) 967-974.
- [7] R. Khoshnavazi, L. Kaviani, F.M. Zonoz, Dioxouranium complexes as ligand. Synthesis and characterization of sandwich-type polyoxometalates  $[\text{X}_2\text{W}_{18}(\text{UO}_2)_2\{(\text{H}_2\text{O})_3\text{M}\}_2\text{O}_{68}]^{10-}$  (X= As<sup>V</sup> and P<sup>V</sup>)(M= Co<sup>II</sup>, Cu<sup>II</sup>, Mn<sup>II</sup>, Ni<sup>II</sup> and Zn<sup>II</sup>), Inorg. Chim. Acta., 362 (2009) 1223-1228.
- [8] J.-W. Zhao, S.-T. Zheng, W. Liu, G.-Y. Yang, Hydrothermal synthesis and structural characterization of two 1-D and 2-D Dawson-based phosphotungstates, J. Solid State Chem., 181 (2008) 637-645.
- [9] V.K. Abdelkader-Fernández, D.M. Fernandes, L. Cunha-Silva, A.J.S. Fernandes, C. Freire, Decorating MOF-74-derived nanocarbons with a sandwich-type polyoxometalate to enhance their OER activity: Exploring the underestimated bulk-deposition approach, Electrochim. Acta 389 (2021) 138719.
- [10] M. Alizadeh, H. Razavi, F.M. Zonoz, M. Mohammadi, Synthesis, single-crystal structural determination and solution characterization of a new sandwich-type cadmium-containing heteropolytungstate, Polyhedron, 22 (2003) 933-939.
- [11] Y. Lin, T.J. Weakley, B. Rapko, R.G. Finke, Polyoxoanions derived from tungstosilicate (A- $\beta$ - $\text{SiW}_9\text{O}_{34}^{10-}$ ): synthesis, single-crystal structural determination, and solution structural characterization by tungsten<sup>183</sup> NMR and IR of titanotungstosilicate (A- $\beta$ - $\text{Si}_2\text{W}_{18}\text{Ti}_6\text{O}_{77}^{14-}$ ), Inorg. Chem., 32 (1993) 5095-5101.
- [12] R. Finke, B. Rapko, T. Weakley, Polyoxoanions derived from A- $\beta$ - $\text{SiW}_9\text{O}_{34}^{10-}$ : synthesis and crystallographic and <sup>183</sup>W NMR characterization of  $[\text{Si}_2\text{W}_{18}\text{Zr}_3\text{O}_{71}\text{H}_3]^{11-}$ , including its organic solvent soluble  $\text{Bu}_4\text{N}^+$  salt, Inorg. Chem., 28 (1989) 1573-1579.
- [13] F. Xin, M.T. Pope, Lone-pair-induced chirality in polyoxotungstate structures: Tin (II) derivatives of a-type  $\text{XW}_9\text{O}_{34}^{10-}$  (X= P, Si). interaction with amino acids, JACS, 118 (1996) 7731-7736.
- [14] K. Wassermann, R. Palm, H.-J. Lunk, J. Fuchs, N. Steinfeldt, R. Stoesser, Condensation of Keggin Anions Containing Chromium (III) and Aluminum (III), Respectively. 1. Synthesis and X-ray Structural Determination of  $[\{\text{A-}\alpha\text{-}\text{SiO}_4\text{W}_9\text{O}_{30}(\text{OH})_3\text{Cr}_3\}_2(\text{OH})_3]^{11-}$ , Inorg. Chem., 34 (1995) 5029-5036.
- [15] U. Kortz, S. Isber, M.H. Dickman, D. Ravot, Sandwich-type silicotungstates: Structure and magnetic properties of the dimeric polyoxoanions  $[\{\text{SiM}_2\text{W}_9\text{O}_{34}(\text{H}_2\text{O})\}_2]^{12-}$  (M= Mn<sup>2+</sup>, Cu<sup>2+</sup>, Zn<sup>2+</sup>), Inorg. Chem., 39 (2000) 2915-2922.
- [16] J. Guo, D. Zhang, L. Chen, Y. Song, D. Zhu, Y. Xu, Syntheses, structures and magnetic properties of two unprecedented hybrid compounds constructed from open Wells-Dawson anions and high-nuclear transition metal clusters, Dalton Trans., 42 (2013) 8454-8459.
- [17] K. Yonesato, H. Ito, H. Itakura, D. Yokogawa, T. Kikuchi, N. Mizuno, K. Yamaguchi, K. Suzuki, Controlled assembly synthesis of atomically precise ultrastable silver nanoclusters with polyoxometalates, JACS, 141 (2019) 19550-19554.

- [18] R. Wang, D. Jia, Y. Cao, Facile synthesis and enhanced electrocatalytic activities of organic-inorganic hybrid ionic liquid polyoxometalate nanomaterials by solid-state chemical reaction, *Electrochim. Acta*, 72 (2012) 101-107.
- [19] K.M. Wiaderek, J.A. Cox, Preparation and electrocatalytic application of composites containing gold nanoparticles protected with rhodium-substituted polyoxometalates, *Electrochim. Acta*, 56 (2011) 3537-3542.
- [20] F.M. Zonoz, F. Aliabadi, A new sandwich-type polyoxometalates containing mixed transition metals,  $[Cd_2Zn_2(H_2O)_2(P_2W_{15}O_{56})_2]^{16-}$ : Syntheses, spectrochemical characterization and its electrocatalytic activity comparison with  $[M_4(H_2O)_2(P_2W_{15}O_{56})_2]^{16-}$  ( $M = Cd^{2+}$  and  $Zn^{2+}$ ) and  $[P_2W_{15}O_{56}]^{12-}$ , *Inorg. Chim. Acta.*, 444 (2016) 87-94.
- [21] A. Bijelic, M. Aureliano, A. Rompel, Polyoxometalates as potential next-generation metallodrugs in the combat against cancer, *Angew. Chem. Int. Ed.*, 58 (2019) 2980-2999.
- [22] H.K. Matthews, C. Bertoli, R.A. de Bruin, Cell cycle control in cancer, *Nat. Rev. Mol. Cell. Biol.*, 23 (2022) 74-88.
- [23] M.R. Sarfjoo, A. Shad, M. Hassanpour, R. Varma, An overview on new anticancer drugs approved by food and drug administration: impending economic and environmental challenges, *Mater Chem Horizons*, 1 (2022) 189-198.
- [24] F. Raza, H. Zafar, A.U. Khan, K. Hatami Kahkesh, T-cell membrane-coated nanomaterials in cancer treatment, *Mater Chem Horizons*, 1 (2022) 199-217.
- [25] F.Z. Amourizi, A.Z. Malek-Khatabi, R. Zare-Dorabei, Polymeric and composite-based microneedles in drug delivery: regenerative medicine, microbial infection therapy, and cancer treatment, *Mater Chem Horizons*, 2 (2023) 113-124.
- [26] A.C. Santos, D. Costa, L. Ferreira, C. Guerra, M. Pereira-Silva, I. Pereira, D. Peixoto, N.R. Ferreira, F. Veiga, Cyclodextrin-based delivery systems for in vivo-tested anticancer therapies, *Drug Delivery and Translational Research*, 11 (2021) 49-71.
- [27] M. Bagherzadeh, M. Safarkhani, H. Daneshgar, F. Radmanesh, F. Taghavimandi, A.M. Ghadiri, M. Kiani, Y. Fatahi, N. Safari-Alighiarloo, S. Ahmadi, N. Rabiee, Magnetic carbon-based nanocomposite decorated with palladium complex for co-delivery of DOX/pCRISPR, *J. Drug Deliv. Technol.*, 78 (2022) 103917.
- [28] A. Mohammadi Zonouz, M. Ghasemzadeh Rahbardar, H. Hosseinzadeh, The molecular mechanisms of ginkgo (*Ginkgo biloba*) activity in signaling pathways: A comprehensive review, *Phytomedicine*, 126 (2024) 155352.
- [29] A. Mohammadi Zonouz, S. Taghavi, S. Nekooei, K. Abnous, S.M. Taghdisi, M. Ramezani, M. Alibolandi, Synthesis of targeted doxorubicin-loaded gold nanorod-mesoporous manganese dioxide core-shell nanostructure for ferroptosis, chemo-photothermal therapy in vitro and in vivo, *Int. J. Pharm.*, 665 (2024) 124725.
- [30] G. Guedes, S. Wang, H.A. Santos, F.L. Sousa, Polyoxometalate composites in cancer therapy and diagnostics, *EurJIC*, 2020 (2020) 2121-2132.
- [31] F. Lu, M. Wang, N. Li, B. Tang, Polyoxometalate-Based Nanomaterials toward Efficient Cancer Diagnosis and Therapy, *Chem. Eur. J.*, 27 (2021) 6422-6434.
- [32] H. Zhao, L. Tao, F. Zhang, Y. Zhang, Y. Liu, H. Xu, G. Diao, L. Ni, Transition metal substituted sandwich-type polyoxometalates with a strong metal-C (imidazole) bond as anticancer agents, *ChemComm*, 55 (2019) 1096-1099.
- [33] R. Francese, A. Civra, M. Rittà, M. Donalisio, M. Argenziano, R. Cavalli, A.S. Mougharbel, U. Kortz, D. Lembo, Anti-zika virus activity of polyoxometalates, *Antivir. Res.*, 163 (2019) 29-33.
- [34] J. Wang, X. Qu, Y. Qi, J. Li, X. Song, L. Li, D. Yin, K. Xu, J. Li, Pharmacokinetics of anti-HBV polyoxometalate in rats, *PLoS One*, 9 (2014) e98292.
- [35] Ş. Bâlici, D. Rusu, E. Páll, M. Filip, F. Chirilă, G.Z. Nicula, M.L. Vică, R. Ungur, H.V. Matei, N.I. Fiț, In Vitro Antibacterial Susceptibility of Different Pathogens to Thirty Nano-Polyoxometalates, *Pharmaceuticals*, 15 (2021) 33.
- [36] A. Bijelic, M. Aureliano, A. Rompel, The antibacterial activity of polyoxometalates: structures, antibiotic effects and future perspectives, *Chem. Commun.*, 54 (2018) 1153-1169.
- [37] N.I. Gumerova, E. Al-Sayed, L. Krivosudský, H. Čipčić-Paljetak, D. Verbanac, A. Rompel, Antibacterial activity of polyoxometalates against *Moraxella catarrhalis*, *Front. Chem.*, 6 (2018) 336.
- [38] T. Hu, Y.-H. Li, X.-F. Kuang, C.-Z. Lu, Synthesis and characterization of polyoxometalate-based silver (i) phenylthynide compounds with antibacterial and antifungal activities, *CrystEngComm*, 19 (2017) 3445-3454.
- [39] K. Rajkowska, A. Koziróg, A. Otlewska, M. Piotrowska, E. Atrián-Blasco, I. Franco-Castillo, S.G. Mitchell, Antifungal activity of polyoxometalate-ionic liquids on historical brick, *Molecules*, 25 (2020) 5663.
- [40] G. Chi, Y. Qi, J. Li, L. Wang, J. Hu, Polyoxomolybdates as  $\alpha$ -glucosidase inhibitors: Kinetic and molecular modeling studies, *J. Inorg. Biochem.*, 193 (2019) 173-179.

- [41] J.J. Hu, L. Wang, B.N. Chen, G.X. Chi, M.J. Zhao, Y. Li, Transition Metal Substituted Polyoxometalates as  $\alpha$ -Glucosidase Inhibitors, *EurJIC*, 2019 (2019) 3270-3276.
- [42] K. Fujinami, K. Dan, T. Tanaka-Kagawa, I. Kawamura, Anti-Aging Effects of Polyoxometalates on Skin, *Appl. Sci.*, 11 (2021) 11948.
- [43] Y. Cheng, K.-J. Qin, D.-J. Zang, Polyoxometalates based nanocomposites for bioapplications, *Rare Met.*, 42 (2023) 3570-3600.
- [44] B. Zhang, J. Qiu, C. Wu, Y. Li, Z. Liu, Anti-tumor and immunomodulatory activity of iron hepta-tungsten phosphate oxygen clusters complex, *Int. Immunopharmacol.*, 29 (2015) 293-301.
- [45] M. Safarkhani, A. Ojaghi, S.M. Nezhad, H. Daneshgar, A.C. Paiva-Santos, F. Radmanesh, M. Bagherzadeh, E.N. Zare, N. Rabiee, P. Makvandi, Engineered (NH<sub>2</sub>)-MIL-125(Ti)/copolymer@MnFe<sub>2</sub>O<sub>4</sub> nanocomposite for synergistic eradication of cancer cells via DOX/pCRISPR delivery, *Adv. Compos. Hybrid Mater.*, 7 (2024) 18.
- [46] A. González, N. Gálvez, M. Clemente-León, J.M. Domínguez-Vera, Electrochromic polyoxometalate material as a sensor of bacterial activity, *ChemComm*, 51 (2015) 10119-10122.
- [47] Y. Sahraoui, S. Chaalia, A. Maaref, A. Haddad, F. Bessueille, N. Jaffrezic-Renault, Mediator enhanced glucose detection using organic-inorganic hybrid supramolecular assembly on gold electrodes, *JEAC*, 781 (2016) 190-197.
- [48] M. Aureliano, N.I. Gumerova, G. Sciortino, E. Garribba, A. Rompel, D.C. Crans, Polyoxovanadates with emerging biomedical activities, *Coord. Chem. Rev.*, 447 (2021) 214143.
- [49] M. Aureliano, The future is bright for polyoxometalates, *BioChem*, 2 (2022) 8-26.
- [50] R. Khoshnavazi, R. Sadeghi, L. Bahrami, High stable sandwich-type polyoxometallates based on A- $\beta$ -SiW<sub>9</sub>O<sub>34</sub><sup>10-</sup>. Synthesis, chemical properties and characterization of [(A- $\beta$ -SiW<sub>9</sub>O<sub>34</sub>)<sub>2</sub> (MOH<sub>2</sub>)<sub>3</sub>CO<sub>3</sub>]<sup>13-</sup> (M= Y<sup>3+</sup> and Yb<sup>3+</sup>), *Polyhedron*, 27 (2008) 1855-1859.
- [51] R.G. Finke, M.W. Droege, P.J. Domaille, Trivacant heteropolytungstate derivatives. 3. Rational syntheses, characterization, two-dimensional tungsten-<sup>183</sup> NMR, and properties of tungstometallophosphates P<sub>2</sub>W<sub>18</sub>M<sub>4</sub> (H<sub>2</sub>O)<sub>2</sub>O<sub>68</sub><sup>10-</sup> and P<sub>4</sub>W<sub>30</sub>M<sub>4</sub> (H<sub>2</sub>O)<sub>2</sub>O<sub>112</sub><sup>16-</sup> (M= cobalt, copper, zinc), *Inorg. Chem.*, 26 (1987) 3886-3896.
- [52] C.J. Gomez-Garcia, E. Coronado, P. Gómez-Romero, N. Casan-Pastor, A tetranuclear rhomblike cluster of manganese (II). Crystal structure and magnetic properties of the heteropoly complex K<sub>10</sub> [Mn<sub>4</sub> (H<sub>2</sub>O)<sub>2</sub> (PW<sub>9</sub>O<sub>34</sub>)<sub>2</sub>]. 20H<sub>2</sub>O, *Inorg. Chem.*, 32 (1993) 3378-3381.
- [53] M.A. Rezvani, A.F. Shojaie, M.H. Loghmani, Synthesis and characterization of novel nanocomposite, anatase sandwich type polyoxometalate, as a reusable and green nano catalyst in oxidation desulfurization of simulated gas oil, *Catal. Commun.*, 25 (2012) 36-40.
- [54] C.M. Tourné, F.T. ° Gilbert, F. Zonnevillage°, Syntheses, Chemical, Structural and Spectroscopic Study, *J. CHEM. Soc. DALTON TRANS*, (1991) 143.
- [55] J.T. Rhule, C.L. Hill, D.A. Judd, R.F. Schinazi, Polyoxometalates in medicine, *Chem. Rev.*, 98 (1998) 327-358.
- [56] J. O'brien, I. Wilson, T. Orton, F. Pognan, Investigation of the Alamar Blue (resazurin) fluorescent dye for the assessment of mammalian cell cytotoxicity, *Eur. J. Biochem.*, 267 (2000) 5421-5426.
- [57] I. Nicoletti, G. Migliorati, M. Pagliacci, F. Grignani, C. Riccardi, A rapid and simple method for measuring thymocyte apoptosis by propidium iodide staining and flow cytometry, *J. Immunol. Methods*, 139 (1991) 271-279.
- [58] Z. Tayarani-Najaran, S. Mousavi, J. Asili, S. Emami, Growth-inhibitory effect of *Scutellaria lindbergii* in human cancer cell lines, *Food Chem Toxicol*, 48 (2010) 599-604.
- [59] L. Chen, D. Shi, J. Zhao, Y. Wang, P. Ma, J. Wang, J. Niu, Three transition-metal substituted polyoxotungstates containing Keggin fragments: from trimer to one-dimensional chain to two-dimensional sheet, *Cryst. Growth Des.*, 11 (2011) 1913-1923.
- [60] T. Yamase, H. Fujita, K. Fukushima, Medical chemistry of polyoxometalates. Part 1. Potent antitumor activity of polyoxomolybdates on animal transplantable tumors and human cancer xenograft, *Inorganica Chim. Acta*, 151 (1988) 15-18.
- [61] F.M. Zonoz, Electrochemistry investigation of the monolacunary and their transition metal substituent Keggin-type polyoxometalates, *Electrocatalysis*, 7 (2016) 215-225.
- [62] Y. Zhou, J. Sun, S. Gallet, J. Raya, C. Boudon, A. Bonnefont, L. Ruhlmann, V. Badets, Nitrite Electroreduction Enhanced by Hybrid Compounds of Keggin Polyoxometalates and 1-Butyl-3-Vinylimidazolium, *ChemCatChem*, 16 (2024) e202400226.
- [63] C.-J. Wang, S. Yao, Y.-Z. Chen, Z.-M. Zhang, E.-B. Wang, Assembly of polyoxometalates and Ni-bpy cationic units into the molecular core-shell structures as bifunctional electrocatalysts, *RSC Adv.*, 6 (2016) 99010-99015.

- [64] I.M. Mbomekalle, B. Keita, Y.W. Lu, L. Nadjo, R. Contant, N. Belai, M.T. Pope, Synthesis and Electrochemistry of the Monolacunary Dawson-Type Tungstoarsenate  $[H_4AsW_{17}O_{61}]^{11-}$  and Some First-Row Transition-Metal Ion Derivatives, *EurJIC*, 2004 (2004) 4132-4139.
- [65] A. Taherian, T. Mazoochi, Different Expression of Extracellular Signal-Regulated Kinases (ERK) 1/2 and Phospho-Erk Proteins in MBA-MB-231 and MCF-7 Cells after Chemotherapy with Doxorubicin or Docetaxel, *Iranian journal of basic medical sciences*, 15 (2012) 669-677.
- [66] X.-B. Xiong, A. Mahmud, H. Uludağ, A. Lavasanifar, Multifunctional polymeric micelles for enhanced intracellular delivery of doxorubicin to metastatic cancer cells, *Pharm. Res.*, 25 (2008) 2555-2566.
- [67] D.C. Wu, C.R. Cammarata, H.J. Park, B.T. Rhodes, C.M. Ofner, Preparation, drug release, and cell growth inhibition of a gelatin: doxorubicin conjugate, *Pharm. Res.*, 30 (2013) 2087-2096.
- [68] N. Tehranian, H. Sepehri, P. Mehdipour, F. Biramijamal, A. Hossein-Nezhad, A. Sarrafnejad, E. Hajizadeh, Combination effect of PectaSol and Doxorubicin on viability, cell cycle arrest and apoptosis in DU-145 and LNCaP prostate cancer cell lines, *Cell Biol. Int.*, 36 (2012) 601-610.
- [69] F. Carvalho, M. Aureliano, Polyoxometalates Impact as Anticancer Agents, *Int. J. Mol. Sci.*, 24 (2023) 5043.
- [70] L. Wang, B.-B. Zhou, K. Yu, Z.-H. Su, S. Gao, L.-L. Chu, J.-R. Liu, G.-Y. Yang, Novel antitumor agent, trilacunary Keggin-type tungstobismuthate, inhibits proliferation and induces apoptosis in human gastric cancer SGC-7901 cells, *Inorg. Chem.*, 52 (2013) 5119-5127.
- [71] I.E. Leon, V. Porro, S. Astrada, M.G. Egusquiza, C.I. Cabello, M. Bollati-Fogolin, S.B. Etcheverry, Polyoxometalates as antitumor agents: bioactivity of a new polyoxometalate with copper on a human osteosarcoma model, *Chem Biol Interact.*, 222 (2014) 87-96.
- [72] J. Luo, G. Jin, F. Zhang, Y. Liu, L. Chen, S. Xie, J. Zhao, Three Types of Mixed Alkali-Metal-, Transition-Metal-, or Rare-Earth-Substituted Sandwich-Type Arsenotungstates with Supporting Rare-Earth Pendants, *EurJIC*, 2018 (2018) 143-152.
- [73] L. Wang, S. Li, Y. Kai, J. Zhu, H. Shi, B. Zhou, J. Liu, The Synthesis and Biological Function of a Novel Sandwich-Type Complex Based on  $\{SbW_9\}$  and Flexible bpp Ligand, *Adv. Healthc. Mater.*, 8 (2019) 1900471.